Assessment of Primary Frequency Control through Battery Energy Storage Systems

Assessment of Primary Frequency Control through Battery Energy Storage Systems

F. Arrigo[a,*], E. Bompard[a], M. Merlo[b], F. Milano[c]

[a]*Department of Energy, Politecnico di Torino, Corso Duca degli Abruzzi 24, Turin, Italy*
[b]*Department of Energy, Politecnico di Milano, Via La Masa 34, Milan, Italy*
[c]*School of Electrical and Electronic Engineering, University College Dublin, Belfield, Ireland*

Abstract

This article focuses on the impact of the primary frequency control that can be provided by Battery Energy Storage Systems (BESSs) on the transient response of electric grids. A procedure based on the Fourier transform is used for synthesizing a realistic frequency signal based on the variations of load consumption and generation. The impact of BESSs is evaluated with respect to the storage capacity installed and the regulation strategy adopted and then compared with the regulation provided by conventional sources. The impact of a variable-droop strategy on the dynamic response of the grid and the BESSs State of Charges (SOCs) is also evaluated. A novel index to quantify the performance of the BESSs is proposed and discussed. The case study is based on a detailed dynamic model of the all-island Irish transmission system.

Keywords: Battery energy storage systems, Fourier transform, frequency control, renewable energy.

1. Introduction

1.1. Motivations

The recent successful operation of a 100 MW BESS installed in South Australia indicates that BESSs are very well suited for Primary Frequency Control (PFC) due to their fast response [1]. In several European systems, BESSs

*Corresponding author
Email address: francesco.arrigo@polito.it (F. Arrigo)

already participate to the PFC service [2] and National Grid in UK has started a new service called "enhanced frequency response" that requires a power response in less than 1 second [3]. This paper addresses the open question of how to assess the performance of BESSs that provide PFC compared to conventional primary frequency controllers during normal grid dynamic conditions. Such an appraisal appears particularly relevant if ancillary services are rewarded proportionally to their effectiveness, as recently recommended by FERC [4].

1.2. Literature Review

There are several studies on the impact of BESSs on primary frequency control. The contribution of BESSs to frequency stability after a contingency is discussed in [5, 6, 7, 8, 9]. The use of BESSs to regulate the frequency within a microgrid is studied in [10, 11]. A third group of studies focuses only on the BESSs without considering their impact on the grid. In these works various strategies, e.g. variable droop, energy arbitrage and participation to balancing markets, are utilised in order to optimize BESS profit and SOC management in addition to frequency regulation. In [12, 13, 14], BESSs regulate their SOC by considering the instantaneous frequency. BESS power output can be adjusted using a different droop, changing the set point when the frequency is in the deadband or considering an over-response from the battery. Heuristic methods [12, 13] or fuzzy control logic [14] is used to control the BESS response. Moreover the use of market schedules and participation in intra-day and balancing markets is considered to avoid over and under charging values [13] and to perform energy arbitrage [14]. More efficient approaches considering dynamic programming are used in [15, 16]. Multi-services provision [17] and the presence of other resources like loads or PV is studied in [18, 19] by using optimization approaches (e.g. model predictive control) in order to maximize the frequency reserve capacity of the BESS. In UK and Central Europe, BESSs are already allowed to vary their droop from the nominal value to partially regulate their SOC [3, 13] by considering a small deviation from the nominal point [12]. Since BESSs capacity devoted to provide PFC service to the grid is expected to in-

crease [1], Variable Droop (VD) strategies are thus expected to play a relevant role.

Multi-hour/day simulations to study the BESSs impact on the grid are considered in [20, 21, 22, 23, 24]. In [20], the impact of a BESS on a small power system is evaluated with field tests by changing the parameters of PFC. The improvement of the frequency signal is estimated by computing the grid frequency standard deviation when BESS is on or off, but not explicitly simulated. In [21], a specific control algorithm that takes into account droop control and SOC management for the BESS is implemented and its effect on the frequency signal is simulated. However, no index is used to quantify this improvement. In [22, 23, 24], the focus is on secondary frequency control, where BESSs are introduced in the simulations to improve the stability of the grid, and their performance is compared to Conventional Generation (CG).

The evaluation of the performance of the frequency control through BESSs is closely linked to the creation of realistic frequency scenarios. In [22, 23, 24], measurement data from several load profiles and photovoltaic power plants are used, while the power exchanged at the tie lines and frequency reserves are estimated. These approaches cannot guarantee a realistic signal, unless a huge and diversified database of measurements is used, which is impractical for large scale power systems. In [21], a system equivalent model is used to reproduce a recorded frequency signal only if real time grid data parameters and variables can be accurately estimated.

The definition of realistic scenarios requires a precise characterization of all components and controllers of the grid. A taxonomy of the frequency variations in Europe is presented in [25]. These are divided into: (i) stochastic frequency deviations due to the fast variations of loads and renewable sources, (ii) deterministic frequency deviations caused by the ramps of CG following their market scheduling [26]. CG undergoes an hourly or sub-hourly unit commitment, which leads to a long term mismatch with respect to the net load [27]. In order to reproduce a realistic signal it is necessary to simulate both typologies of frequency deviations and verify the resulting variability of the frequency signal

with real-world data.

1.3. Contributions

The contributions of this paper are as follows:

- quantify the impact of the primary frequency control provided by BESSs and compare it to CG contribution through the use of a novel quantitative index. It is also studied the impact of a VD control strategy used by BESSs.
- a novel procedure, whose preliminary version appeared in [28], to generate realistic synthetic frequency scenarios.

1.4. Organization

The remainder of the paper is organized as follows. Section 2 presents the stochastic models included in the grid, whereas Section 3 describes the adopted frequency control of the BESS. Section 4 outlines the procedure to create realistic scenarios. Section 5 describes various indexes, included the proposed one, to evaluate the performance of the control provided by BESSs and other energy resources. Section 6 describes the case study and discusses simulation results. Finally, Section 7 provides conclusions and outlines future work.

2. Modelling of Stochastic Processes

In normal dynamic conditions, frequency variations are mostly determined by the unbalance between total produced and consumed power [29]. This unbalance is caused by the variations of loads, wind power plants and conventional generators ramping to change set point. Power variations are stochastic and, thus, a proper mechanism to emulate randomness has to be put in place to obtain realistic results from simulations. We provide below a short description of the devices involved in the creation of the power disturbances considered in this work.

2.1. Conventional Generation

The PFC of conventional power plants is shown in Fig. 1. f_{nom} is the nominal frequency of the grid, while f is the instantaneous frequency value, p_{pfc} is the power requested by primary frequency control, p_{ord} is the power reference set point of the turbine and R [pu(Hz)/pu(MW)] is the droop of the controller. The lead-lag block represents the turbine governor dynamics and p_m is the mechanical output of the turbine. By changing the time constants it is possible to simulate different CG technologies like steam, gas and hydro power plants. The model is detailed enough for transient stability studies, where frequency variations remain well bounded and the focus is the overall response of the system. As explained in Section 4, p_{ord} is subjected to ramps of maximum amplitude $|\Delta p_{\max}|$ with time period Δt_{CG} ranging from few minutes up to one hour in order to mimic the power variations yielded by net load following dispatching. In such a way, we reproduce slow power fluctuations around the net load. An example of such fluctuations is shown in Fig. 2.

2.2. Load

Load models are assumed to be voltage-dependent, i.e., exponential or ZIP models, and either static or dynamic voltage recovery [30]. The reference power consumption of a load, say p_{load}, is defined as the sum of two components:

$$p_{\text{load}} = p_{\text{det}} + p_{\text{sto}} \ , \tag{1}$$

where p_{det} is the "deterministic" consumption which is assumed to vary linearly between assigned values in a given period, e.g. 15 minutes; p_{sto} is a stochastic

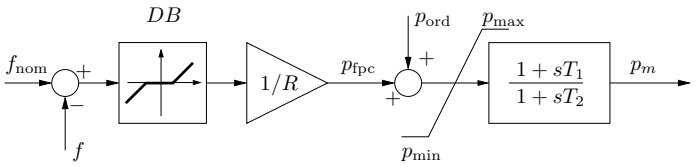

Figure 1: simplified model of the primary frequency control and turbine of conventional power plants. Note that all quantities in the figure are in pu.

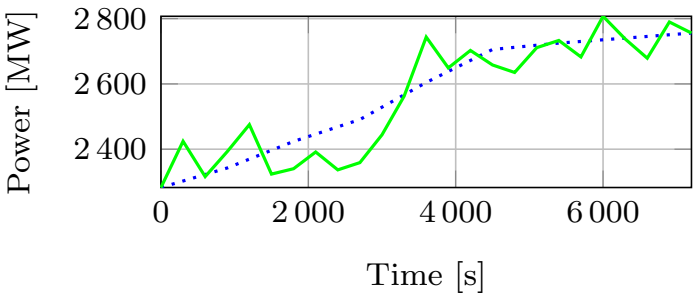

Figure 2: example of noise that reproduces slow fluctuations. The blue dotted line represents the net load, while the green solid line represents the net load plus CG fluctuations.

fluctuation that models volatility. p_{sto} is defined as a Gaussian distribution with a given standard deviation σ_{Load}. Stochastic variations are computed with a given period Δt_i. Fig. 3 shows an example of load profiles.

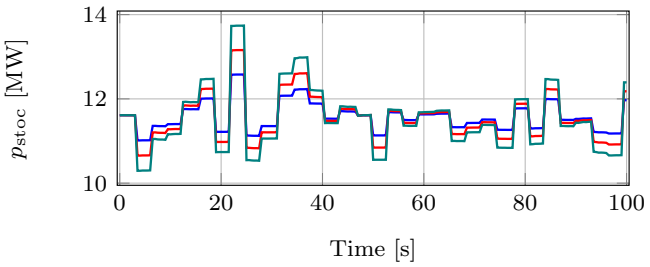

Figure 3: examples of p_{sto} profiles using $\Delta t_i = 3$ s and various standard deviations, namely 2.5, 4 and 5.5%.

2.3. Wind Generation

Wind generators are modelled as doubly-fed induction generators (Type C). The turbine is fed by wind speed time series, which are defined as the sum of two components: wind speed stochastic component $w_{\text{s,sto}}$ $[m/s]$ and $w_{\text{s,ramp}}$ $[m/s]$ component modelled as linear wind speed ramps with a certain time period. The stochastic component is modelled as a set of Stochastic Differential Equations (SDEs) based on the Ornstein-Uhlenbeck Process [31], also known as mean-

reverting process. The equations for the wind speed ω_s can be written as follows:

$$w_s = w_{\text{s,ramp}} + w_{\text{s,sto}} \ , \tag{2}$$

$$\dot{w}_{\text{s,sto}} = \alpha(\mu_w - w_{\text{s,sto}}) + b_w(\sigma_w)\xi_w \ , \tag{3}$$

α is the mean reversion speed that dictates how quickly the $w_{\text{s,sto}}$ tends to the given mean value μ_w (in our case 0). ξ_w is the white noise, formally defined as the time derivative of the Wiener process. This process is controlled by adjusting α and the standard deviation σ_w of the wind stochastic part which affects the b_w component. Fig. 4 shows three sample wind stochastic profiles obtained by changing the σ_w and α parameter.

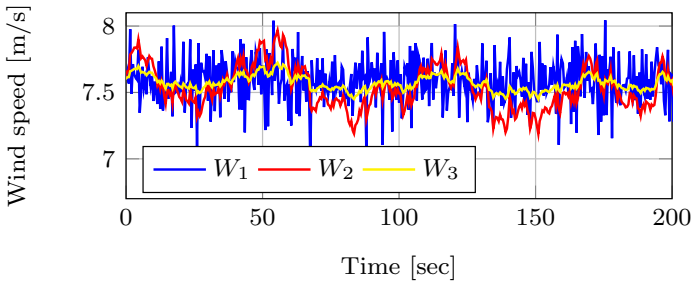

Figure 4: $w_{\text{s,sto}}$ profiles. W_1 ($\alpha = 10$, $\sigma_w = 0.17$); W_2 ($\alpha = 0.1$, $\sigma_w = 0.17$); W_3 ($\alpha = 0.1$, $\sigma_w = 0.06$).

3. BESS Control

In this study, we consider the BESS model defined in [32]. The power produced by the battery is transferred to the grid through a current source converter. The converter includes the PI controllers that regulate the active and reactive powers at the point-of-connection with the ac grid. Overall the BESS responds within a second after a Δp request. The reference active power is defined by the PFC control. Two PFC characteristics are considered in this study, namely fixed and variable droop control strategy. The latter is a novel contribution of this paper.

3.1. Fixed Droop (FD)

This control is implemented as a fixed power/frequency curve, as commonly in use for CG. The droop (R) of CG plants is usually set at 0.04 or 0.05 pu considering a 10% regulation band of the generator nominal power, as specified in the Irish grid code [33]. Depending on these parameters, a certain frequency error $\Delta f_{\max}$ causes the full provision of the regulation band. In general the droop for a CG and a BESS unit is computed as follows [34]:

$$R_{\mathrm{CG}} = \left| -\frac{\Delta f_{\max}}{f_{\mathrm{nom}}} \cdot \frac{1}{PFC_{\mathrm{band}}^{\mathrm{CG}}} \right| , \tag{4}$$

$$R_{\mathrm{BESS}} = \left| -\frac{\Delta f_{\max}}{f_{\mathrm{nom}}} \cdot \frac{1}{PFC_{\mathrm{band}}^{\mathrm{BESS}}} \right| , \tag{5}$$

where PFC_{band} represents the regulator band in pu (in this study, we set $PFC_{\mathrm{band}}^{\mathrm{CG}} = 0.1$ pu(MW) and $PFC_{\mathrm{band}}^{\mathrm{BESS}} = 1$ pu(MW)). Taking $\Delta f_{\max}$ equal for both resources and dividing equation (5) by (4), we obtain the relationship which correlates both the droops:

$$R_{\mathrm{BESS}} = R_{\mathrm{CG}} \cdot \frac{PFC_{\mathrm{band}}^{\mathrm{CG}}}{PFC_{\mathrm{band}}^{\mathrm{BESS}}} = R_{\mathrm{CG}} \cdot 0.1 \ . \tag{6}$$

For each value of the CG droop one obtains a corresponding BESS droop which saturates its regulation band at the same frequency deviation of the CG resources.

3.2. Variable Droop (VD)

Frequency fluctuations distribute symmetrically around f_{nom} and follow a normal distribution or a binomial one if a deadband in governors controller of CG is present [35]. Therefore, the PFC of the battery usually works on average 50% in under-frequency and 50% over-frequency periods with a zero mean energy. However, using a FD frequency control characteristic, due to the internal losses of the battery the SOC is expected to gradually decrease to 0. At the same time, long over-frequency periods could make the BESS reach maximum SOC, limiting its regulation capacity. The proposed VD strategy tries to avoid such extreme SOC conditions by introducing an asymmetry in the frequency control of the BESS.

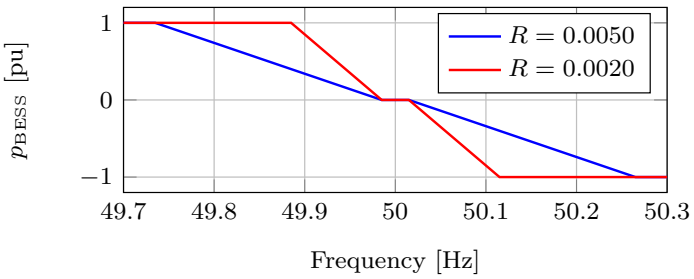

Figure 5: Power limits example for the VD frequency control.

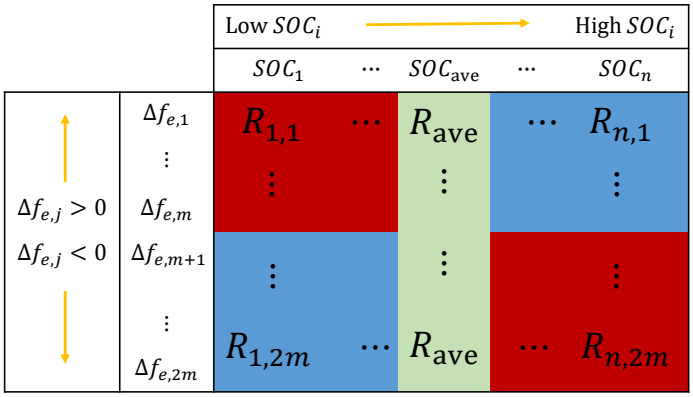

Figure 6: VD lookup table scheme.

As shown in Fig. 5, we assume that the droop is variable and bounded by two values, namely $R_{\max}$ and $R_{\min}$. These values are limited by system stability and resources technical considerations. Usually TSOs request droop values between 2 and 8% [36], typical values are 4 and 5%.

The VD is implemented through the use of a two dimensional lookup table, where the droop value depends on the instantaneous frequency error $\Delta \text{f}_\text{e} = \text{f}_\text{nom} - \text{f}$ and the SOC. The droop values are divided in five different areas (see Fig. 6): (i) in the red areas the values are close to $R_{\max}$, (ii) in the blue areas the values are close to $R_{\min}$ and (iii) in the green area (which correspond to a column vector) the droop values are all equal to the average droop R_{ave}, at half distance between $R_{\max}$ and $R_{\min}$. The values of the table are therefore constructed symmetrically in such a way that the BESS is expected to avoid

excess discharge or charge keeping its SOC close to SOC_{ave} level. As an example, if SOC is high and Δf_e is positive then the BESS discharges with a low droop to reach SOC_{ave}, whereas if Δf_e is negative it charges with a high droop to slow down the SOC increase.

Note that, in order to regulate the SOC the best choice would be to set the droop values equal to $R_{\max}$ in red areas and $R_{\min}$ in blue areas. However, to avoid sudden droop changes and less effective frequency regulation, droop values gradually approach $R_{\max}$ and $R_{\min}$.

A better SOC regulation is achieved by setting the SOC_i values close to SOC_{ave} and taking small values of $\Delta f_{e,j}$. Better SOC management is also expected if the distance between the maximum and minimum droop $R_{\max}$ and $R_{\min}$ is large.

The VD strategy here proposed cannot achieve a perfect SOC regulation being a decentralized technique, nevertheless it is useful to improve the SOC dynamics with respect to a FD strategy and it is used in this study to make the BESS droop change realistically during the simulations and analyse the impact of VD strategies on the grid frequency stability.

4. Generation of Realistic Scenarios

Our aim is now to reproduce realistic frequency fluctuations in order to properly quantify the BESS contribution to the PFC. The reference scenario, considered below, is a time series of the frequency measured by the authors at University College of Dublin. The data represents 330 days of measurements with a sampling rate of 10 Hz.

A Discrete Fourier Transform (DFT) is applied to define the harmonic content of the frequency measurements. The goal is to synthetize and then simulate a dynamic base case scenario (S1) with a harmonic content similar to the real frequency data sampled in the lab. The implemented procedure is valid to replicate the harmonic amplitudes of six hours of real frequency signal. Of all the thousands of harmonics computed through the DFT, only the first 800 are

considered, which represent more than the 98% of the variance of the signal for all the days considered (as computed by applying Parseval's Theorem). The frequency signal is therefore a "slow" signal in that the first harmonics (characterized by longer periods) hold more importance than the shorter period ones. For example, in Fig. 7 we show the harmonic profiles related to the six hour period going from 6:00 to 12:00, the mean μ and the standard deviation σ of each harmonic for all days considered. All the profiles are similar. The grid frequency signal is therefore quite variable in time domain but much more similar in the harmonic content. Therefore, to reproduce similar harmonic amplitudes of the real data assures that the synthetic signal behaves realistically. Similar results hold for the other three time ranges (00:00-6:00, 12:00-18:00, 18:00-24:00).

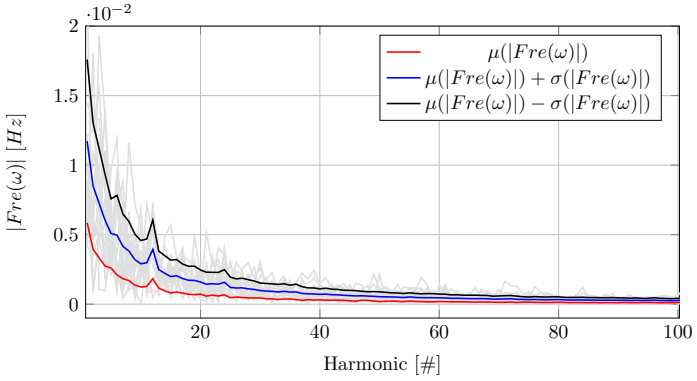

Figure 7: harmonics amplitudes related to the six hour period 6:00-12:00.

In order to reproduce real data harmonics, we make use of power stochastic profiles from generation and consumption. These processes are divided in two groups following the taxonomy presented in the literature review, as follows:

- *Fast Stochastic Processes (FSP).* The stochastic processes of load consumption and wind speed discussed in Section 2 are used to replicate the events that cause stochastic frequency fluctuations in the grid (typically with period lower than 2 minutes).

- *Slow Stochastic Processes (SSP).* Two noises are used to model determin-

istic frequency deviations: SSP1 which models wind and CG ramps and SSP2 which models the long term mismatch between net load and conventional generation due to the market structure of the system. SSP1 are noises up to 10 minutes, while SSP2 are up to one hour. We refer to these deviations as slow frequency variations.

To tune the parameters of each component of FSP and SSP, a precise mapping between stochastic processes and excited frequency harmonics is defined and stored in a database. This is obtained by varying the parameters values, simulating the grid and then computing and recording the resulting harmonic amplitude. To separate the effect of each stochastic process, one perturbation at a time is considered, being null all other stochastic processes. The parameters used to variate the stochastic processes are the ones described in Section 2 and are a total of 7.

In particular, for the load model, a variety of time periods Δt_i (going from 0.5 to 2 seconds) and standard deviations σ_{Load} (going from 2 to 15%) values are considered. σ_w is the only parameter to be changed to vary the stochasticity of the wind component with α fixed to 0.1. For the SSP, time steps and power ramps are chosen from uniform distributions with specified limit values. In the case of SSP1, time steps Δt_{CG} go from 2 to 10 minutes, while for SSP2 the period goes from 13 to 60 minutes. In the case of power variations, requested ramps are both negative or positive, with a maximum $|\Delta p_{\max}|$ which goes from 10 MW up to 70 MW for both SSP noises.

Figures 8 and 9 show several harmonic profiles obtained from the simulation of FSP and SSP noises. As expected, The former noises excite short period harmonics, while the latter give rise exclusively to long period harmonics.

Finally, the stochastic processes of loads, wind speeds and CG power set points are summed together and the resulting profile, say p_{tot}, is thus identified by a given unique set of parameters that define the four stochastic processes. The harmonic contents of the frequency trajectories obtained with p_{tot} are then compared with the real data through the estimation of an error ϵ_f, which is

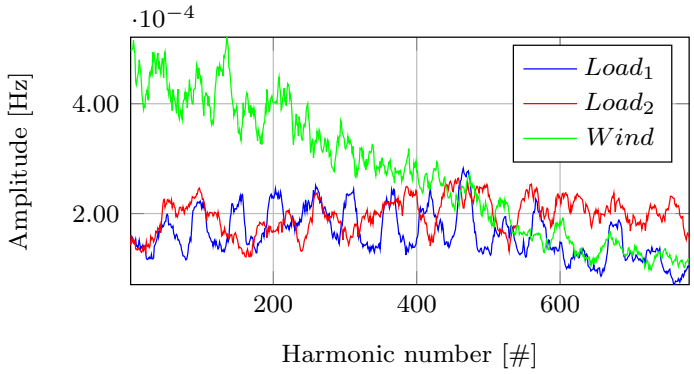

Figure 8: examples of harmonic obtained with load and wind stochastic processes. $Load_1$ ($\Delta t_i = 1s,\ \sigma_{\text{Load}} = 2\%$); $Load_2$ ($\Delta t_i = 0.5s,\ \sigma_{\text{Load}} = 2\%$); Wind ($\sigma_w = 3\%$).

defined as follows:

$$\epsilon_i = \begin{cases} |(Y\text{sim}_\text{i} - (\text{Yreal}_\text{i} - \text{std}_\text{i}))|, & \text{if } Y\text{sim}_\text{i} < (\text{Yreal}_\text{i} - \text{std}_\text{i}), \\ (Y\text{sim}_\text{i} - (\text{Yreal}_\text{i} + \text{std}_\text{i})), & \text{if } Y\text{sim}_\text{i} > (\text{Yreal}_\text{i} + \text{std}_\text{i}), \\ 0, & \text{if } (Y\text{real}_\text{i} - \text{std}_\text{i}) < \text{Ysim}_\text{i} < (\text{Yreal}_\text{i} + \text{std}_\text{i}) \end{cases} \tag{7}$$

$$\epsilon_f = \frac{\sum_{i=1}^{N_\text{harm}} \epsilon_i}{\sum_{\text{i}=1}^{\text{N}_\text{harm}} \text{Yreal}_\text{i}} \tag{8}$$

where ϵ_i is the error at the harmonic i; $Y\text{sim}_\text{i}$ is the value of the simulated frequency data at the harmonic i; $Y\text{real}_\text{i}$ is the mean of all real data at the harmonic i; std_i is the standard deviation of the real frequency data at the harmonic i; N_harm is the number of harmonic used.

If this error falls within the desired tolerance, the procedure ends, otherwise relevant noise parameters are increased or decreased according to their impact on the signal harmonics. In such a way the procedure creates a scenario in which frequency does not emulate a specific real day data, but it tries to recover the average variability of real measurements. The synoptic scheme that illustrates the procedure is shown in Fig. 10.

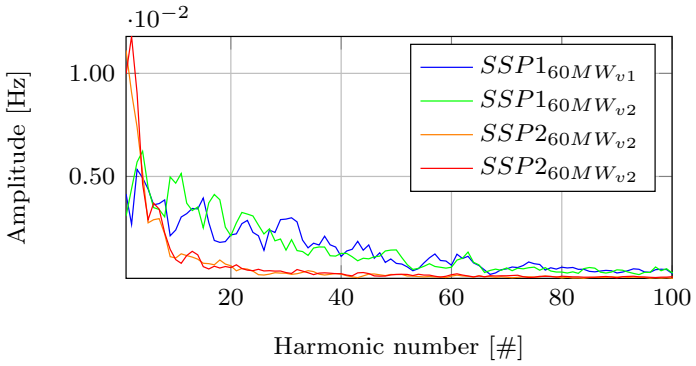

Figure 9: examples of harmonic groups obtained with the SSP1 and SSP2 noises. $v1$ and $v2$ refer to different noise profiles with equal $|\Delta p_{\max}|$ value. Δt_{CG} is equal to 3-7 minutes for SSP1 and 13-50 minutes for SSP2.

5. Indexes

This section describes a variety of indexes that allow evaluating the impact of stochastic processes and the effectiveness of the PFC provided by BESSs and CG.

5.1. Impact of the stochastic processes on the system dynamic response

To quantify the contribution of each stochastic process to the overall frequency fluctuations, we consider the sum variance law of the frequency signal which defines the variance of a signal composed by N stochastic independent variables as:

$$\sigma^2_{\mathrm{TOT}} = \sum_{i=1}^{N} \sigma_i^2 \ . \tag{9}$$

To compare the impact of each process, it is convenient to consider a normalized variance per process, namely:

$$\sigma^2_{i,\mathrm{pu}} = \frac{\sigma_i^2}{\sigma^2_{\mathrm{TOT}}} \ , \tag{10}$$

in such a way, from Equ. (9), we can write:

$$1 = \sum_{i=1}^{N} \sigma^2_{i,\mathrm{pu}} \ . \tag{11}$$

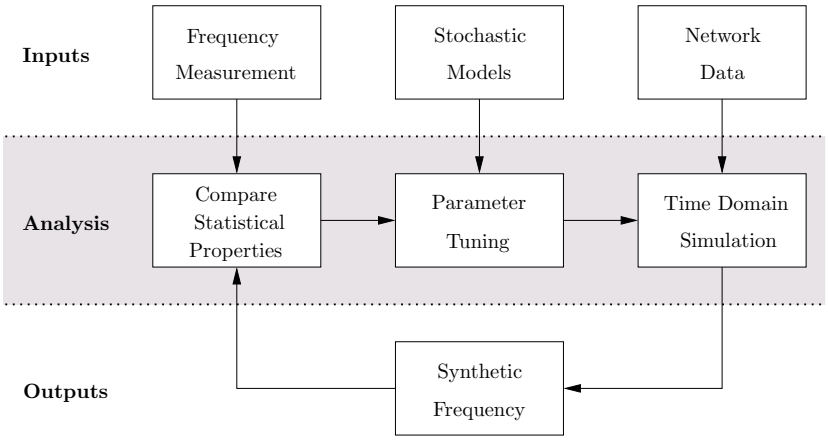

Figure 10: Procedure to generate realistic scenarios.

5.2. Impact of BESSs on frequency fluctuations

This index provides a measure of the relative improvement to the dynamics response due to the BESSs. It is defined as:

$$h_{\mathrm{B}} = 1 - \frac{\sigma_{\mathrm{B}}}{\sigma_o} \ , \tag{12}$$

where σ_{B} is the standard deviation of the frequency of the system with inclusion of BESSs and σ_o is the standard deviation of the frequency for the same scenario but without BESSs.

5.3. Effectiveness of the PFC

This novel proposed index evaluates the effectiveness of the frequency control provided by any resource included in the system. Considering a resource k, the index is defined as:

$$e_k = \frac{E_k^+ + \left|E_k^-\right| - (E_{o,k}^+ + \left|E_{o,k}^-\right|)}{E_k^{\mathrm{ref}}} \ , \tag{13}$$

where

$$E_k^{\mathrm{ref}} = \int_o^T \frac{P_{\mathrm{nom,k}}}{R_k(r)} \left|\Delta f(r)\right| dr \ . \tag{14}$$

R_k [pu] is the droop of the resource which, for the BESS regulated with VD, is a time-dependent quantity, $P_{\mathrm{nom,k}}$ [MW] is the nominal power of the resource

and $|\Delta f(r)|$ [Hz] is the frequency error including the deadband. E_k^{ref} represents the integral of the exact real-time power profile requested by the PFC service in a given period T, E_k^+ represents the actual energy produced by the resources for $\Delta f > 0$, whereas E_k^- is the energy produced for $\Delta f < 0$ in the same period T. The condition $E_k^+ + E_k^- < E_k^{\text{ref}}$ generally holds as E_k^+ and E_k^- account for the delays of the primary frequency control dynamics. $E_{o,k}^+$ and $\left|E_{o,k}^-\right|$ represent the energy produced for $|\Delta f| < db$ where db is the deadband of the controller. These energies work against the PFC requirements and thus reduce the effectiveness of the frequency control.

According to the above definition, $e_k = 0$ if the resource does not participate to PFC, $e_k \ll 1$ if the resource is slow and not able to follow the PFC reference signal and $e_k = 1$ for an ideal frequency control with instantaneous time response.

6. Case Study

This case study discusses the performance of the BESS PFC decribed in Section 3 and its impact on various scenarios based on the procedure discussed in Section 4. With this aim, we make use of the Irish transmission system [37]. Table A.5 in the appendix summarizes the main elements of the grid. The CG active installed capacity in S1 is 4347 MW while wind active installed capacity is 2123 MW. In S2 and S3 CG capacity is decreased by 25%.

All simulations are solved using Dome [38], a Python and C-software based tool that allows simulating large scale power systems modelled as a set of stochastic differential algebraic equations. Relevant components are modelled in detail such as a high voltage network topology, a 6-th order machine model of the synchronous generator, frequency and voltage regulators etc.

6.1. Scenarios Construction

Three scenarios, S1, S2 and S3, are considered. In Appendix A we report the static and dynamic parameters of the CG PFC.

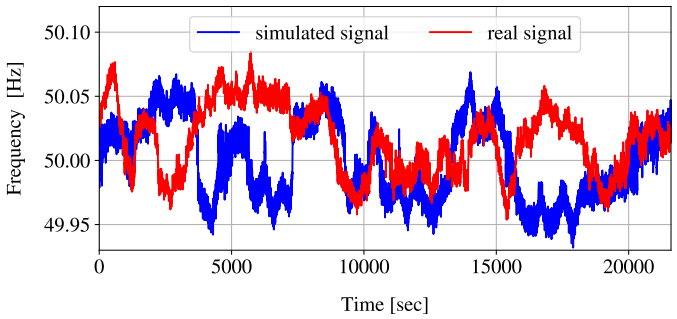

Figure 11: comparison between real and simulated (S1) frequency

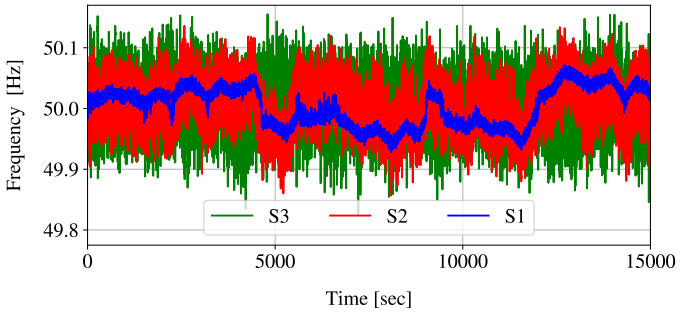

Figure 12: frequency profiles examples for the three considered scenarios.

The time horizon of the three scenarios is 12 hours, from 6:00 to 18:00. Load and wind linear slow power profiles are defined based on real-world data obtained by the Irish TSO Eirgrid, while the mismatch from the net load comes from the application of the 4 noises presented in Section 4.

Each scenario is first simulated without the BESSs. S1 represents the scenario that reproduces the measurement data obtained in the lab. S2 and S3 include higher level of noises and decreasing inertia levels, which lead to greater and faster frequency fluctuations. In particular, in S2 we increase the FSP noises and decrease the SSP2 noise, while in S3 the SSP noises are reduced almost to zero and FSP noises are highly increased.

One profile of scenario S1 and a real frequency time series are shown in Fig. 11. As expected, the synthetic frequency signal retains a similar variability

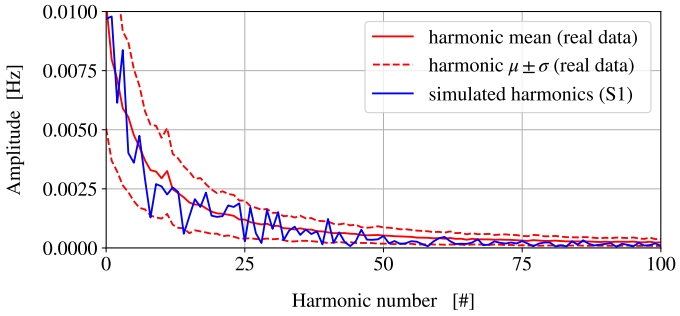

Figure 13: harmonic comparison between simulated and real data for the scenario S1, period 12:00 - 18:00.

with respect to the real data. Sample frequency fluctuations of the three scenarios are shown in Fig. 12. Table 1 summarizes the standard deviation of the frequency of the system σ_f, the normalized variances $\sigma^2_{i,\mathrm{pu}}$ of the four stochastic components and the two S1 errors ϵ_f evaluated by applying Equ. (8). In S1 (real-world scenario) the slow noises (SSP) represent almost 90% of the grid deviations with more than half coming from SSP2 noises. In S2 and S3, SSP2 noise goes towards zero. The noises parameters which were used to create the scenarios can be seen in Table B.8 in Appendix B. Note that in both this table and table 1 values of S2 ans S3 were computed as the average between the two six hours time periods.

In Fig. 7 the harmonics of real data and S1 scenario are compared and as expected from the definition of error ϵ_f, the simulated profile is well bounded by the real data harmonics standard deviation. Moreover the mean of the signal in the scenarios is set in accordance with the mean of the 330 real days. For this reason, frequency signal is slightly under 50 Hz for the first 6 hours and over 50 Hz for the period from 12:00 to 18:00. These frequency mean offsets are very important in order to capture day frequency dynamics which affect the BESS SOC profiles.

Table 1: normalized variances and frequency standard deviations for the three stochastic scenarios

Scenario #	σ_f [Hz]	μ_f [Hz]	$\sigma^2_{i,\text{pu}}$				ϵ_f [pu]
			Load	$Wind_{\text{sto}}$	SSP_1	SSP_2	
S1 (6:00-12:00)	0.0308	49.9996	0.09	0.02	0.34	0.55	0.032
S1 (12:00-18:00)	0.0302	50.0038	0.075	0.07	0.34	0.515	0.021
S2 (6:00-18:00)	0.0359	50.0028	0.22	0.12	0.37	0.29	-
S3 (6:00-18:00)	0.0431	50.0021	0.55	0.24	0.16	0.05	-

6.2. BESS Frequency Control

The simulations that include BESSs are divided in two groups: the first considers exclusively the dynamic behaviour of FD, the second compares FD and VD control strategies. For the first group, the three scenarios are simulated by considering four BESS capacities (100, 200, 300 and 400 MW) and three droop values ($R_{BESS} = 0.005, 0.004, 0.0035$). In the second group, S1 and S2 scenarios are simulated, with 100, 200 and 300 MW of BESSs characterized by two efficiencies ($\eta_{\text{BESS}} = 0.8, 0.9$) and by a power-energy ratio equal to 0.4.

With regard to the PFC, two FD droops (equal to 0.004 and 0.0035) are compared respectively to two VD strategies which are shown in Table 2: (i) "hard mode", for which the droop varies in the range $R \in [0.002, 0.005]$, and (ii) "soft mode", for which the droop varies in the range $R \in [0.003, 0.005]$. The tables have been built following the process described in Section 3.2 considering 4 SOC_i and 4 $\Delta f_e, j$ points. For both modes $SOC_{\text{ave}} = 60\%$, while R_{ave} is equal to 0.004 in the hard mode and 0.0035 in the soft mode which are the values used by the FD strategy. Both setups, especially hard mode, make the droop to vary significantly during the simulations in order to regulate the SOC as well as possible.

Table 2: lookup tables for VD "hard" and "soft" control modes. Note that droop is here expressed in % and not in pu to improve readability of values.

Hard mode					**Soft mode**				
Δf_e	SOC range				Δf_e	SOC range			
[Hz]	50%	55%	60%	70%	[Hz]	45%	50%	60%	75%
0.03	0.20	0.20	0.35	0.50	0.040	0.3	0.35	0.40	0.50
0.0175	0.20	0.25	0.35	0.50	0.020	0.35	0.375	0.40	0.50
-0.0175	0.50	0.45	0.35	0.20	-0.020	0.45	0.425	0.40	0.30
-0.03	0.50	0.50	0.35	0.20	-0.040	0.50	0.45	0.40	0.30

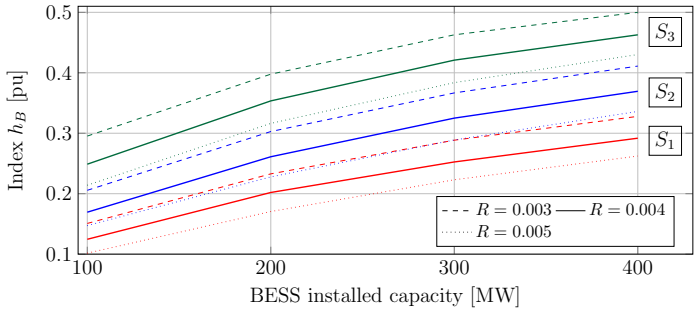

Figure 14: index h_{B} for the FD control strategy of the BESSs. The droop values is indicated by R. Different colors represents different scenarios.

6.2.1. FD control strategy

Fig. 14 shows the index h_{B} for the various scenarios. The improvement of the frequency signal is more relevant for both scenarios S2 and S3 (see Fig. 15 for an example) than for S1. This has to be expected as, in S1, frequency has smaller standard deviation closer to the deadband value, which limits the impact of BESSs. For similar reasons, as shown Fig. 14, the h_{B} index increments tend to decrease as BESS capacity increases.

Table 3 shows the index e_k for the available resources that provide PFC. In the table, only one value for each scenario and each resource is shown, as e_k is

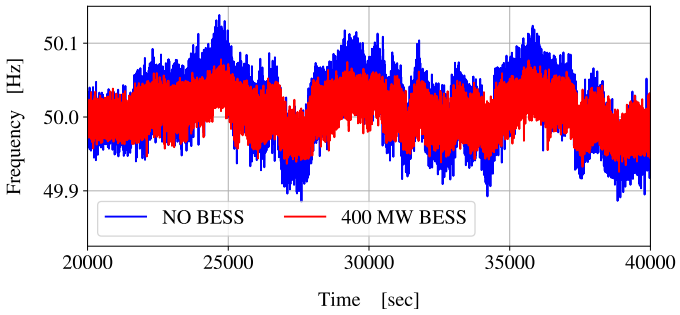

Figure 15: frequency profiles for scenario S2 without BESS and with BESS.

Table 3: index e_k for various scenarios and energy resources

Device	S1	S2	S3
BESS	0.99	0.99	0.97
Steam	0.92	0.78	0.31
Hydro	0.94	0.84	0.44
Gas	0.99	0.98	0.89

not greatly affected by the BESS installed capacity and its droop value. Two parameters mostly influence the index e_k:

- *The time response of the resource.* A fast time response of the resource improves its frequency regulation. As an example Fig. 16 shows the active power outputs of the BESS and of a conventional steam power plant. The blu dotted line is the reference PFC signal to be followed by the two resources. The fast response of the BESS leads to an almost perfect tracking of the reference signal.

- *The harmonic content of the frequency fluctuations.* The index e_k of the conventional power plants is higher in scenarios S1 and S2 than S3 in that the frequency signal is slower and easier to follow even for slower resources.

The result of the simulations is that in scenario S1, which represents the

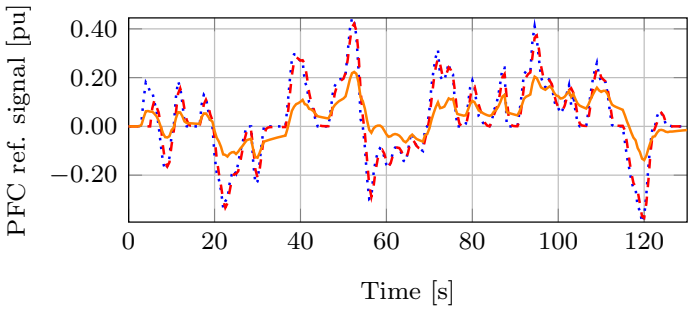

Figure 16: power production of the BESS (dashed red line) and of CG (solid orange line) following a PFC reference signal (dotted blue line).

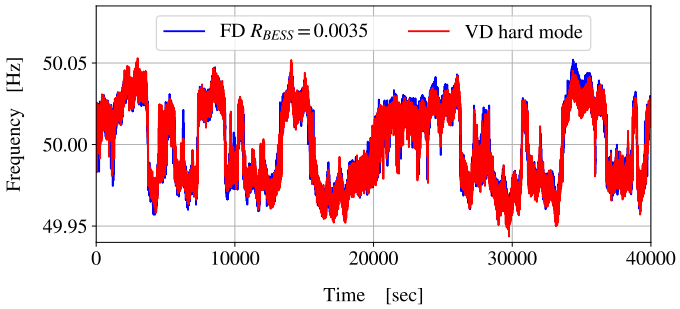

Figure 17: frequency profiles examples with FD and VD strategy ($\eta_{\mathrm{BESS}} = 0.8$) adopted and 200 MW BESS installed.

current situation, the performance of the BESSs is comparable with that of conventional power plants. In S2 and S3, which are characterized by faster frequency fluctuations, the regulation provided by BESSs have much more value than CG PFC service.

6.2.2. VD control strategy

In order to asses the impact of VD strategies, several standard statistical properties of the frequency signal are used. Note that only the results with $\eta_{\mathrm{BESS}} = 0.8$ are shown. The cases with $\eta_{\mathrm{BESS}} = 0.9$ provide similar results and thus are here neglected. In the case of VD strategies, the standard deviation of the frequency signal has a negligible difference in the order of 10^{-4} Hz

Table 4: relevant parameters of simulations related to the case $\eta_{\mathrm{BESS}} = 0.8$

Sim.	Par.	VD_{hard}	$FD_{0.35}$	VD_{soft}	$FD_{0.4}$
	$\sigma(fre)$	0.0239	0.02393	0.02444	0.02443
$S1_{200\mathrm{MW}}$	Skew(fre)	-0.1004	-0.0662	-0.0821	-0.722
	$\mu(SOC)$	0.57	0.58	0.56	0.54
	$\sigma(fre)$	0.0223	0.02235	0.02285	0.02286
$S1_{300\mathrm{MW}}$	Skew	-0.143	-0.118	-0.122	-0.12
	$\mu(SOC)$	0.59	0.61	0.59	0.62
	$\sigma(fre)$	0.02595	0.02581	0.02655	0.02648
$S2_{200\mathrm{MW}}$	Skew	0.143	0.066	0.0938	0.0722
	$\mu(SOC)$	0.63	0.70	0.63	0.69
	$\sigma(fre)$	0.02349	0.02342	0.02418	0.02416
$S2_{300\mathrm{MW}}$	Skew	0.142	0.04	0.131	0.042
	$\mu(SOC)$	0.63	0.66	0.63	0.64

with respect to the FD strategies. In Fig. 17 we can visualize the frequency signal of selected simulations which show great similarity. As shown in Table 4, VD strategies generally enlarge skewness, creating small asymmetries in the frequency signal. If the initial skewness is negative, the VD strategies will further lower this value, while the opposite is true in case the initial skewness is positive. The difference is bigger in the case of hard mode with respect to soft mode and when BESS installed capacity is higher, except for the case $S1_{300\mathrm{MW}}$. In general two compensating effects happen as BESS capacity increases: on one hand, as SOC diverges from the nominal SOC_{ave} value, the droop fluctuates around R_{ave}. This dynamic is responsible for creating the asymmetries in the frequency signal and increases its impact as more BESSs are used. On the other hand, the big BESS capacity makes the frequency less variable and closer to the deadband limiting the impact of VD strategies.

For these reasons the differences in the frequency signal remain small in the order of 10^{-1} [pu] and the values of skewness are still quite close to 0 and therefore do not represent a big distortion. Finally, in both scenarios, the kurtosis slightly increase in the order of 10^{-3} [pu].

It is therefore clear that little difference exist between VD and FD strategies even if a large BESS capacity is installed. Both strategies are enough to guarantee stability in the grid during normal dynamic conditions.

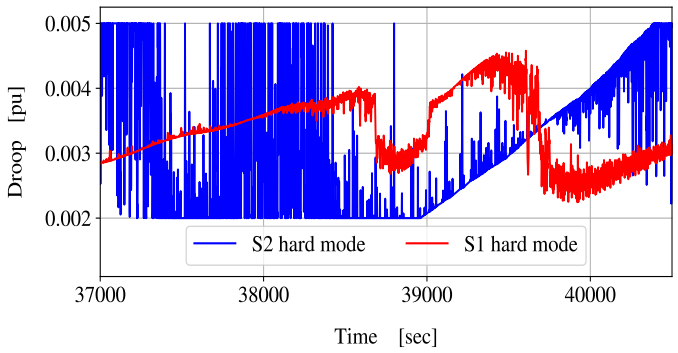

Figure 18: example of droop profiles in S2 with 100 MW of BESS installed and $\eta_{\mathrm{BESS}} = 0.8$

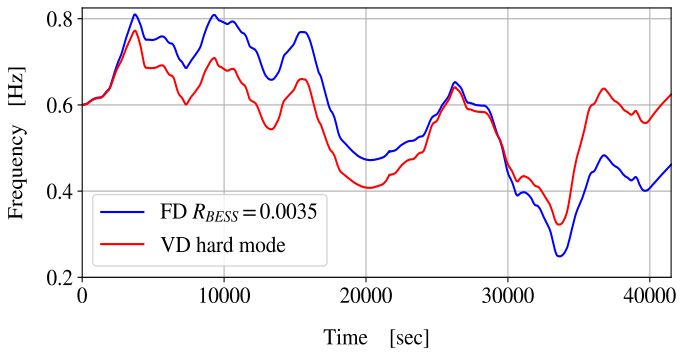

Figure 19: example of SOC profiles in the S1 scenario with 100 MW of BESS installed

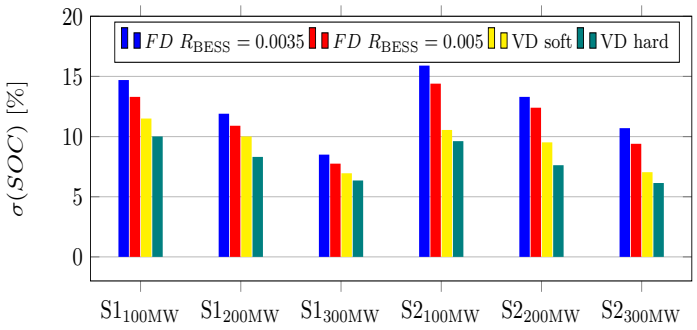

Figure 20: index $\sigma(SOC)$ for various BESS control strategies and capacities with $\eta_{\mathrm{BESS}} = 0.8$.

For what concerns SOC, in Table 4 the mean SOC value $\mu(SOC)$ of several simulations is shown. VD strategies, especially for S2, are able to keep the SOC statistically closer to SOC_{ave} with respect to FD strategies. Fig. 19 shows as an example two profiles related to the different strategies. As can be seen, the VD strategy is not able to perfectly regulate the SOC, but manages to decrease its standard deviation with respect to the FD case avoiding too high or too low charge levels. Fig. 20 shows the SOC standard deviation for all the scenarios studied in the case $\eta_{BESS} = 0.8$. The decrease in standard deviation is slightly better in S2 where the alternation between over and under-frequency periods is faster, therefore the VD strategy changes values often (as shown

in Fig. 18), reaching better performances. The possibility of using a bigger difference between $R_{\max}$ and $R_{\min}$ can further improve the SOC dynamics (e.g. $R_{\min} = 0.002$ and $R_{\max} = 0.008$), but its effect on the frequency must be carefully evaluated.

7. Conclusions

In this paper we have studied the potential impact of BESSs on the PFC of power systems. Realistic scenarios are generated through a technique that properly reproduces load and generation variations based on the the DFT. Simulation results confirm that BESSs can reduce the fluctuations of the frequency provided that they are properly controlled and enough capacity is installed. The effectiveness of the frequency support is quantified by means of an effectiveness index e_k.

The performance of the BESS control depends both on the amount of inertia and the nature of frequency deviations present in the system. If the inertia is high and frequency fluctuations are caused by slow phenomena (as currently happen), the performance of the BESSs is similar to that of fast turbine governors. As inertia decreases and more stochastic fast noises are present into the grid (for example due to the increase of renewable sources) the BESSs are more effective than the conventional primary frequency controllers of synchronous machines (even more than doubling the performance of slow thermal plants). Finally, variable droop control strategy does not seem to impact signal standard deviation and just marginally modify the frequency stability with respect to the fixed droop case, while at the same time improves the BESS SOC management.

Future work will be focused on a more rigorous assessment of the impact of variable droop control discussed in the paper by considering more scenarios, parameters and different regulation laws.

Acknowledgment

This work has been developed as part of the activities of RESERVE European project, grant agreement No. 727481.

Federico Milano is funded by Science Foundation Ireland (SFI), through the Investigator Programme, under award AMPSAS, Grant No. SFI/15/IA/3074. The opinions, findings and conclusions or recommendations expressed in this material are those of the authors and do not necessarily reflect the views of the SFI.

The authors would like to thank Eng. Ferdinando Parma, Eng. Massimo Pozzi and Dr. Davide Falabretti for their help in this work.

Appendix A. Grid static and dynamic characteristics

Table A.5: Main elements of the transmission system used

Network	#	Loads and Power Plants	#
AC Power Lines	796	Loads	346
Bus	1479	Conventional Generators	22
Transformers	1055	Wind power plants	472

Table A.6: Parameters of primary and secondary frequency control

Primary Control	Reserve [MW]	Band Reserved [%]	Droop [%]	Deadband [mHz]
S1	421	10	5	15
S2 & S3	302	10	5	15

Table A.7: Parameters of the turbine governors of conventional generators

Time Constant	Steam	Hydro	Gas
T_1 [s]	10	2.5	0.5
T_2 [s]	3	0	0

Appendix B. Noises parameters of the Scenarios

Table B.8: Stochastic noises parameters values used to create the scenarios

Scenario #	Load		Wind	SSP1		SSP2	
	Δt_i [s]	σ_{Load} [%]	σ_w [%]	Δt_{CG} [min]	$\Delta p_{\max}$ [MW]	Δt_{CG} [min]	$\Delta p_{\max}$ [MW]
S1 (6:00-12:00)	0.5	2.75	2.5	3-6	33	13-50	50
S1 (12:00-18:00)	0.5	3	5	4-7	38	15-50	47.5
S2 (6:00-18:00)	0.5	8.5	12.5	3.5-6.5	39	14-50	22.5
S3 (6:00-18:00)	0.5	16	25	4-7	20	14-50	10

Bibliography

[1] Kempener R, Borden E. Battery storage for renewables: market status and technology outlook. International Renewable Energy Agency, Abu Dhabi, 2015.

[2] ENTSO-E. Consultation Report "FCR Cooperation"; 2017.

[3] National Grid. National Grid frequency services, https://www.nationalgrideso.com/balancing-services/frequency-response-services/enhanced-frequency-response-efr; 2019 [accessed 4 June 2019].

[4] Order no. 755: Frequency regulation compensation in the organized wholesale power markets. Federal Energy Regulatory Commission, Washington DC, 2011.

[5] Ramírez M, Castellanos R, Calderón G, Malik O. Placement and sizing of battery energy storage for primary frequency control in an isolated section of the Mexican power system. Elec Power Syst Res 2018;160:142-150. https://doi.org/10.1016/j.epsr.2018.02.013.

[6] ENTSO-E. Frequency stability evaluation criteria for the synchronous zone of continental Europe; 2016.

[7] Ortega Á, Milano F. Modeling, simulation, and comparison of control techniques for energy storage systems. IEEE Trans Power Syst 2017;32(3):2445-54. https://doi.org/10.1109/TPWRS.2016.2602211.

[8] Ortega Á, Milano F. Stochastic transient stability analysis of transmission systems with inclusion of energy storage devices. IEEE Trans Power Syst 2018;33(1):1077-79. https://doi.org/10.1109/TPWRS.2017.2742400.

[9] Toma L, Sanduleac M, Baltac SA, Arrigo F, Mazza A, Bompard E et al. On the virtual inertia provision by BESS in low inertia power systems. In: IEEE International Energy Conference (ENERGYCON) 2018, pp.1-6. https://doi.org/1109/ENERGYCON.2018.8398755.

[10] Zhao H, Hong M, Lin W, Loparo KA. Voltage and frequency regulation of microgrid with battery energy storage systems. IEEE Trans Smart Grid 2019;10(1):414-24.10. https://doi.org/1109/TSG.2017.2741668

[11] Aghamohammadi MR, Abdolahinia H. A new approach for optimal sizing of battery energy storage system for primary frequency control of islanded microgrid. Int J Elec Power 2014;54,325-33. https://doi.org/10.1016/j.ijepes.2013.07.005.

[12] Oudalov A, Chartouni D, Ohler C. Optimizing a battery energy storage system for primary frequency control. IEEE Trans Power Syst 2007; 22(3),1259–66. https://doi.org/10.1109/TPWRS.2007.901459.

[13] Thien T, Schweer D, vom Stein D, Moser A, Sauer D U. Real-world operating strategy and sensitivity analysis of frequency containment reserve provision with battery energy storage systems in the German market. J. Energy Storage 2017;13:143-63. https://doi.org/10.1016/j.est.2017.06.012

[14] Brivio C, Mandelli S, Merlo M. Battery energy storage system for primary control reserve and energy arbitrage. Sustainable Energy, Grids Netw 2016;6:152–65. https://doi.org/10.1016/j.segan.2016.03.004.

[15] Zhang YJA, Zhao C, Tang W, Low SH. Profit-maximizing planning and control of battery energy storage systems for primary frequency control. IEEE Trans Smart Grid 2016;9(2):712-23. https://doi.org/10.1109/TSG.2016.2562672.

[16] Cheng B, Powell W B. Co-optimizing battery storage for the frequency regulation and energy arbitrage using multi-scale dynamic programming. IEEE Trans Smart Grid 2016;9(3):1997-2005.

[17] Engels J, Claessens B, Deconinck G. Combined stochastic optimization of frequency control and self-consumption with a battery. IEEE Trans Smart Grid 2017;10(2):1971-81.

[18] Namor E, Sossan F, Cherkaoui, R, Paolone M. Control of battery storage systems for the simultaneous provision of multiple services. IEEE Trans Smart Grid 2018;10(3):2799-808.

[19] Mégel J, Mathieu J L, Andersson G. Scheduling distributed energy storage units to provide multiple services under forecast error. Int J Elect Power Energy Syst 2015;72:48–57.

[20] Stein K, Tun M, Matsuura M, Rocheleau R. Characterization of a fast battery energy storage system for primary frequency response. Energies 2018; 11(12) 3358. https://doi.org/10.3390/en11123358.

[21] Jo H,Choi J, Agyeman KA, Han S. Development of frequency control performance evaluation criteria of BESS for ancillary service: a case study of frequency regulation by KEPCO. In: IEE Innovative Smart Grid Technologies-Asia Conference (ISGT-Asia) 2017, pp.1-5. https://doi.org/10.1109/ISGT-Asia.2017.8378437

[22] Cheng Y, Tabrizi M, Sahni M, Povedano A, Nichols D. Dynamic available AGC based approach for enhancing utility scale energy storage performance. IEEE Trans Smart Grid 2014;5(2):1070-78. https://doi.org/10.1109/TSG.2013.2289380.

[23] Chen S, Zhang T, Gooi HB, Masiello RD, Katzenstein W. Penetration rate and effectiveness studies of aggregated BESS for frequency regulation. IEEE Trans Smart;7(1):167-77. https://doi.org/10.1109/TSG.2015.2426017.

[24] Zhang F, Hu Z, Xie X, Zhang J, Song J. Assessment of the effectiveness of energy storage resources in the frequency regulation of a single-area power system. IEEE Trans Power Syst;32(5):3373-80. https://doi.org/10.1109/TPWRS.2017.2649579.

[25] ENTSO-E, EURELECTRIC. Deterministic frequency deviations–root causes and proposals for potential solutions; 2011.

[26] ENTSO-E. Continental Europe Significant Frequency deviations; 2011.

[27] Remppis S, Gutekunst F, Weissbach T, Maurer M. Influence of 15-minute contracts on frequency deviations and on the demand for balancing energy. In: International ETG Congress 2015, pp.1-7.

[28] Arrigo F, Merlo M, Parma F. Fourier transform based procedure for investigations on the grid frequency signal. In: Innovative Smart

Grid Technologies Conference Europe (ISGT-Europe) 2017, pp.1-6. https://doi.org/10.1109/ISGTEurope.2017.8260312.

[29] Anderson PM, Fouad AA. Power system control and stability. 2nd ed. John Wiley & Sons; 2008.

[30] Milano F. Power System Modelling and Scripting. London:Springer; 2010.

[31] Zárate-Miñano R, Anghel M, Milano F. Continuous wind speed models based on stochastic differential equations. Appl Energy 2013;104:42-9. https://doi.org/10.1016/j.apenergy.2012.10.064

[32] Milano F, Ortega Á. Converter-Interfaced Energy Storage Systems. London: Cambridge University Press; 2019.

[33] Eirgrid. Irish Grid Code. http://www.eirgridgroup.com/site-files/library/EirGrid/GridCodeVersion6.pdf; 2015 [accessed 4 June 2019]

[34] Kundur P, Balu NJ, Lauby MG. Power system stability and control. New York: McGraw-Hill; 1994.

[35] Mele FM, Ortega Á, Zárate-Miñano R, Milano F. Impact of variability, uncertainty and frequency regulation on power system frequency distribution. In: Power Systems Computation Conference (PSCC-Genoa) 2016, pp.1-6. https://doi.org/10.1109/PSCC.2016.7540970

[36] Terna. Italian grid code, attachment A15: load frequency control participation, https://download.terna.it/terna/0000/0105/32.pdf; 2008 [accessed 4 June 2019]

[37] EirGrid and SONI. All-island ten year transmission forecast statement; 2017.

[38] Milano F. A Python-based software tool for power system analysis. IEEE Power & Energy Society General Meeting 2013, pp.1-5. https://doi.org/10.1109/PESMG.2013.6672387.

547